Analysis of Seismic Data from the Shumagin Seismic Gap, Alaska

14-08-0001-G1981

Geoffrey A. Abers, Klaus H. Jacob
Lamont-Doherty Geological Observatory of Columbia University
Palisades, New York 10964
(914) 359-2900

Nontechnical Summary

The largest known earthquakes occur in subduction zones, but relatively little is known about their faulting processes.We use observations of moderate earthquakes from a dense network in the East Aleutians to gain understanding of the physical processes that control their rupture and, by extension, that control rupture of larger earthquakes. We are determining the mode of faulting of earthquakes away from the main thrust zone, to better understand the regional stress state. New methods are developed for comparing small and large earthquakes, to quantify rupture histories of the large events and to look for spatial or temporal changes in faulting modes.

Analysis of Seismic Data from the Shumagin Seismic Gap, Alaska

14-08-0001-G1981

Geoffrey A. Abers, Klaus H. Jacob
Lamont-Doherty Geological Observatory of Columbia University
Palisades, New York 10964
(914) 359-2900

Investigations

The mechanics of rupture on plate boundary faults remain poorly understood, but play a critical role in the nucleation and extent of major earthquakes. This is particularly true of subduction zones, where little local seismic data exist. The Shumagin network has recorded 10 years of digital seismic data within 0-100 km of the main Aleutian interplate thrust, with a variety of types of instruments. We analyze here the spatial distribution, mechanisms, and rupture processes of small-to-moderate (M<5) earthquakes, by using the local network seismic data. A primary task is to use empirical Green's function techniques to remove path effects in waveforms of moderate-sized earthquakes, by deconvolving from these seismograms the waveforms of small earthquakes from the same location and with the same mechanism. The resulting wavelets reflect the source behavior of the larger earthquakes, and can be quantified using a variety of standard measures (e.g., seismic moment, radiated seismic energy, duration, directivity, stress drop). We explore these measures and their variation between different parts of the main thrust zone, in order to document variations in the mechanical behavior of the interplate thrust. We are testing the possibility that variations exist between shallow and deep parts of the thrust zone, following the suggestion from teleseismic analyses that deeper earthquakes (40-50 km depth) have much higher stress drops than shallower events (25-35 km) closer to the trench. As a parallel part of this study, we analyze the spatial variability of seismicity and earthquake properties in regions near the main interplate thrust zone, in order to gain insight into the stress field at a subduction zone and of mechanical differences between the interplate thrust and the surrounding region.

Results

1. A compilation of instrument response characteristics and polarities over time has been completed. This information is a necessary first step to quantitative analysis of earthquake size and signal frequency content. Previously unknown instrument characteristics were measured during the 1991 Shumagin field season, estimated from particle-motion studies, or determined from laboratory calibrations following the network removal (see report in this volume for cooperative agreement #14-08-0001-A0616, Seismic Monitoring of the Shumagin Seismic Gap, Alaska). Some strong differences existed from previously-used, nominal values. Several discrepancies were documented in horizontal-component orientation (checked with particle motion analysis), non-standard telemetry component gains (checked in laboratory tests, only a problem for two stations), and seismometer free periods (nominal 1 Hz instruments exhibited free periods varying from 0.9 Hz to 1.6Hz). A data-base is nearly completed for the period of digital recording, 1982-1991.

2. Redetermined ray parameters, together with new picks, have been used to determine single-event fault plane solutions from Shumagin data. Ray parameters have been redetermined for the larger earthquakes using rays traced through a recently-determined laterally-varying velocity model, using the exact ray-tracing scheme used in the velocity inversion. Preliminary work has been done on shallow upper plate events, which provide evidence on the state of stress in the subduction zone and its mode of deformation. Results for upper-plate events (Figure 1) show both strike-slip and thrust mechanisms, in all cases with *P*-axes roughly perpendicular to the direction of plate convergence (one M=1.5 normal-faulting event occurred as an aftershock 33 minutes after a M=4.6 mainshock, and is not thought to represent long-term tectonic deformation). These earthquakes are all less than 20 km deep, and overlie both the interplate thrust zone and the deeper part of the descending seismic zone (Figure 1C). These mechanisms suggest that the maximum horizontal stress is perpendicular, rather than parallel to the arc in the forearc.

3. Two new methods have been developed for determining source pulses and rupture durations from empirical Green's function (EGF) data. The first method is direct inversion of the seismogram pairs for source duration. We assume a simple source model, such as a boxcar, ramp, or a "Brune" ($kte^{-t/D}$) source pulse parameterization (Figure 2A), and directly invert seismograms for the duration and amplitude of the pulse. Although the inversion is nonlinear the number of parameters being sought is small (one, usually), so fully nonlinear inversions are feasable. These inversions directly incorporate estimates of the uncertainties due to the model and due to the simplified parameterization, and calculate *a posteriori* probabilities for all values of source duration. The result is a complete nonlinear probability density function for source duration, which is used to investigate confidence limits (e.g., Figure 2B,C). Because the number of parameters are very small the method is usually robust, and provides a direct estimate of desired measures of the earthquake source. The method is being extended to incorporate multiple stations for the same event pair, and to determine rupture directivity as well average duration (a three parameter problem). The example shown in Figure 2 shows ~50% variations in duration between stations for a given rupture model, although the variation does not depend on a simple way with either distance or azimuth.

The second method is a time-domain deconvolution of EGF events from seismograms for larger earthquakes (Figures 3,4). In this approach the convolution of an EGF with a source pulse is directly inverted for the source pulse time series, similar to least-squares deconvolution methods used in seismic reflection processing. An inverse operator is constructed from the EGF seismogram, incorporating *a priori* estimates of uncertainties in the large event seismogram, the Green's function, and in the source pulse. The time-domain formalism allows *a priori* uncertainty estimates to be introduced in a natural way, and the strictly linear nature of the problem allows reasonable uncertainties and resolution estimates to be made. We find that small amounts of stabilization are considerably more effective using this procedure than using frequency-domain methods, allowing us to determine source pulses more reliably and for more events.

This approach has been found to be considerably more robust with respect to nonstationary errors in the Green's function (i.e., decreasing reliability of the Green's function with time into the record. In the synthetic-seismogram example shown on Figure 3, the phase of late arrivals seismograms is changed by increasing the depth 0.2 km. Increasing phase incoherence with time in the seismogram is often observed, and usually dealt with by careful windowing or selection of seismogram pairs by ad hoc visual comparisons of coherence. The time-domain inversions are able to correctly reproduce the early part of the seismogram that are not affected by EGF phase errors, because inversion for the early part of the seismogram is to first order independent of the later, incoherent part. By contrast, the frequency-domain inversion result is contaminated at all times. Similarly, deconvolution "errors" due to seismogram truncation produce relatively larger errors in the source pulse for frequency-domain deconvolutions than time-domain deconvolutions, even when the otherwise correct Green's function is used.

An example using Shumagin network data is shown in Figure 4. This data is recorded digitally at 100 samples per second with 12-bit samples, the sensors have a flat velocity response between ~1 Hz and 30 Hz. The same pair of events is used as in Figure 2, both aftershocks of a M=4.6 upper-plate event in May, 1988. Resolution effects are shown by plotting rows of the resolution matrix corresponding to three representative times in the source pulse (Figure 4C, E). For the single-seismogram inversion the width of the resolution peak is 0.04-0.05 s and the peak becomes broader with increasing lag. These peak-widths are a significant fraction of the 0.15 s observed pulse duration, and suggest that finite resolution width may provide a minimum bound on observable source durations. A frequency-domain approach would not improve matters, as low-pass filtering and other stabilizers will also limit resolution of the source duration. One way around this problem is to invert several seismograms simultaneously for the same event-EGF pair (Figures 4D,E); the redundancy introduced here makes the resolution rows much more peak-like, at least for small lags. The primary difficulty with this approach is that duration is assumed constant at all stations, and directivity effects are ignored. For metrics such as stress drop that require a single source duration, the joint inversion probably provides a reasonable estimate.

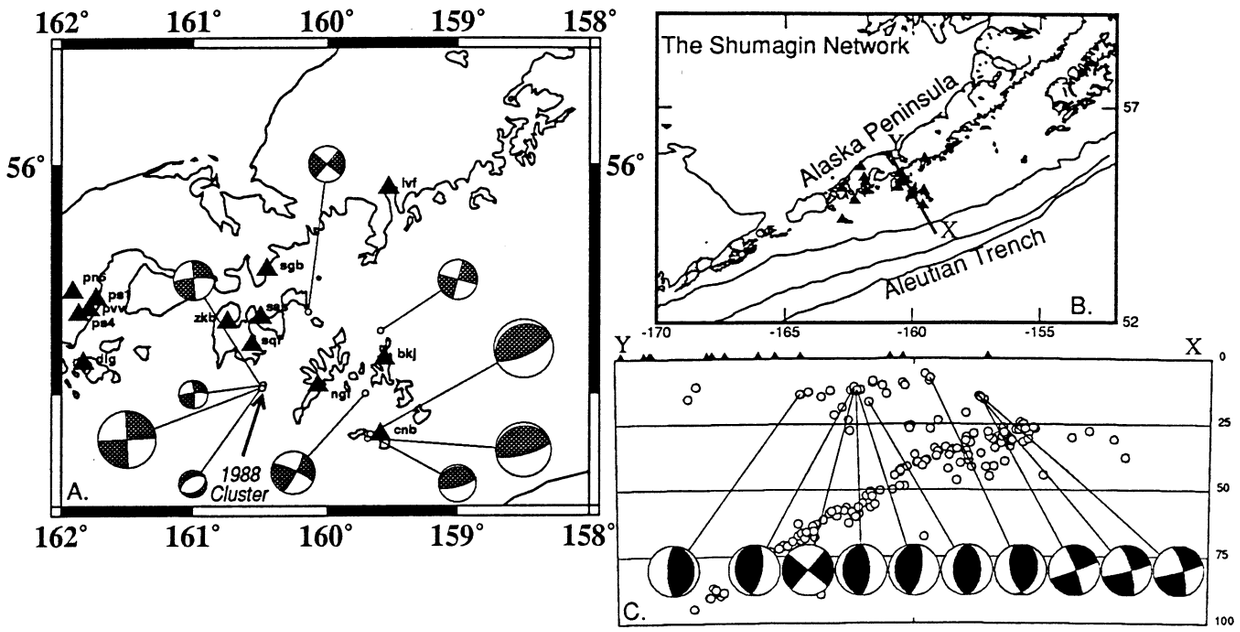

Figure 1. Fault-plane solutions for shallow, upper-plate earthquakes in the Shumagin Islands region determined from first motions. Fault plane solutions are determined for individual events, using ray parameters determined from exact ray-tracing through 3D velocity model. A. Map showing mechanisms and station locations. Fault-plane solutions are plotted as lower-hemisphere projections, and radii are scaled to magnitude (magnitudes range from 1.5 to 4.7). B. Location map, Y-X is cross-section location. C. Cross-section of seismicity. Depths in km at right. Earthquakes are relocated in 3D model; only stable locations are plotted. Fault-plane solutions are plotted in a back-hemisphere projection. Triangles show station locations, projected onto section.

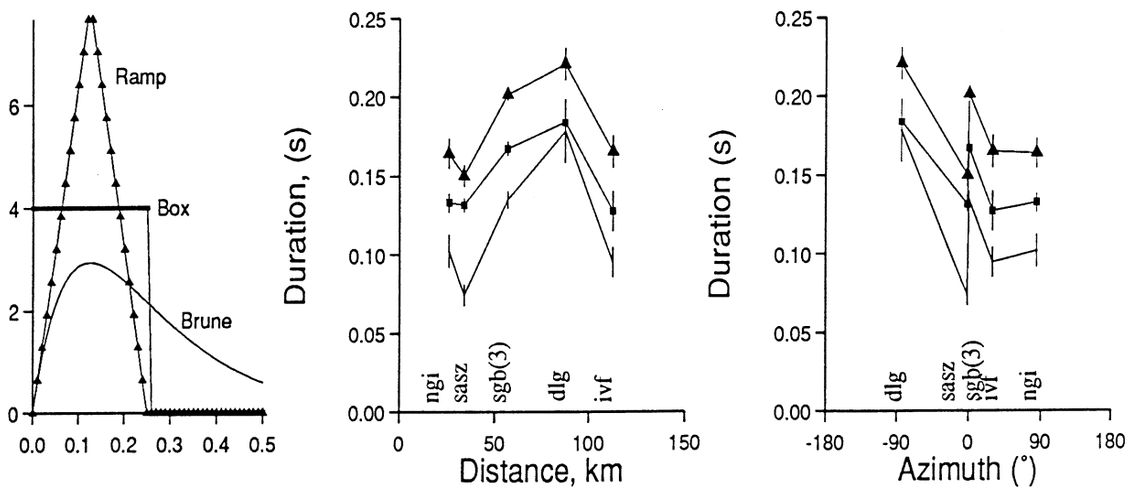

Figure 2. Single-parameter inversions for source duration. A. Shape of characteristic pulses used; all have 0.25s duration or 0.125s rise-time. B. Results for deconvolution of EGF for event in 1988 Cluster (Fig. 1A, Fig. 4) vs. distance of station; same stations as Fig. 4. Symbols are for different source models: triangle, ramp; square, box; none, "Brune". C. Same as B, plotted vs. azimuth to station. Calculation described in text. Errors are one-sigma, calculated from second moment of a posteriori probability density functions for pulse duration.

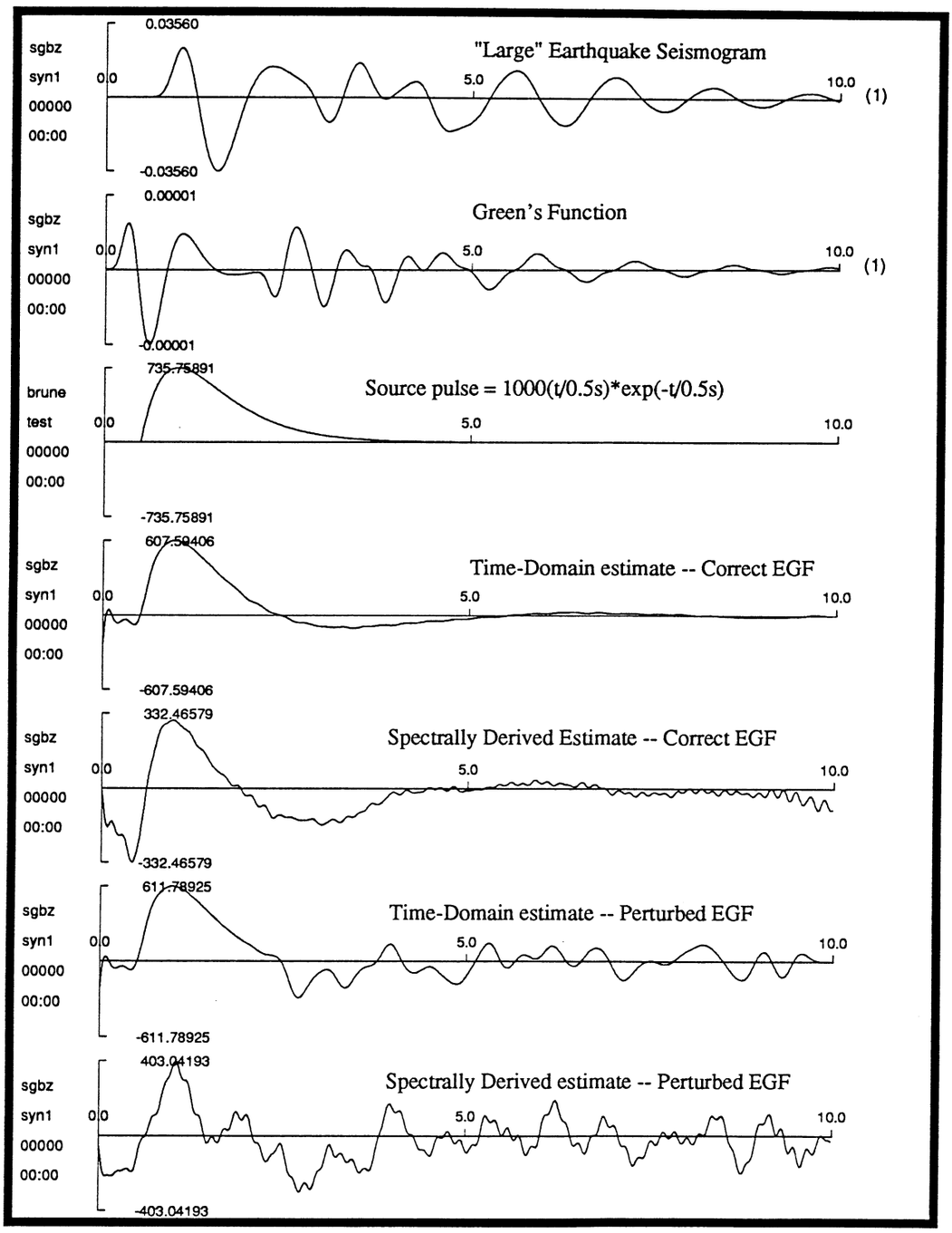

Figure 3. Tests of empirical Green's function (EGF) deconvolution using synthetic seismograms. The true Green's function TGF (second record) was calculated as a teleseismic event recorded by Shumagin network short-period sensors (flat response to velocity, 1-30 Hz). The receiver-structure was half-space, assumed source-region structure was 0.5 km thick water-layer over half space. Other parameters for TGF: source depth 2.5 km, ray parameter 0.08 s/km (for 30° distance), attenuation parameter t*=0.6 s; source duration of 0.01 s; thrust mechanism with 45°-dipping planes striking parallel to ray azimuth. The top seismogram was generated by convolving the TGF with the source pulse shown third from top. Fourth record is result of time-domain deconvolution of the top record from TGF, assuming a priori uncertainties typical of real data. The fifth record is the result of doing the same deconvolution by taking the ratio of complex spectra, low-pass filtering the result at 6.25 Hz, 1/4 the Nyquist frequency, with a 6-pole Butterworth filter. The bottom two source pulse estimates were made in the same way as the fourth and fifth records, except that a perturbed EGF was used. The perturbed EGF was calculated identically to the TGF, except the source depth was increased by 200 meters, resulting in phase errors at lag times greater than 2.0 s.

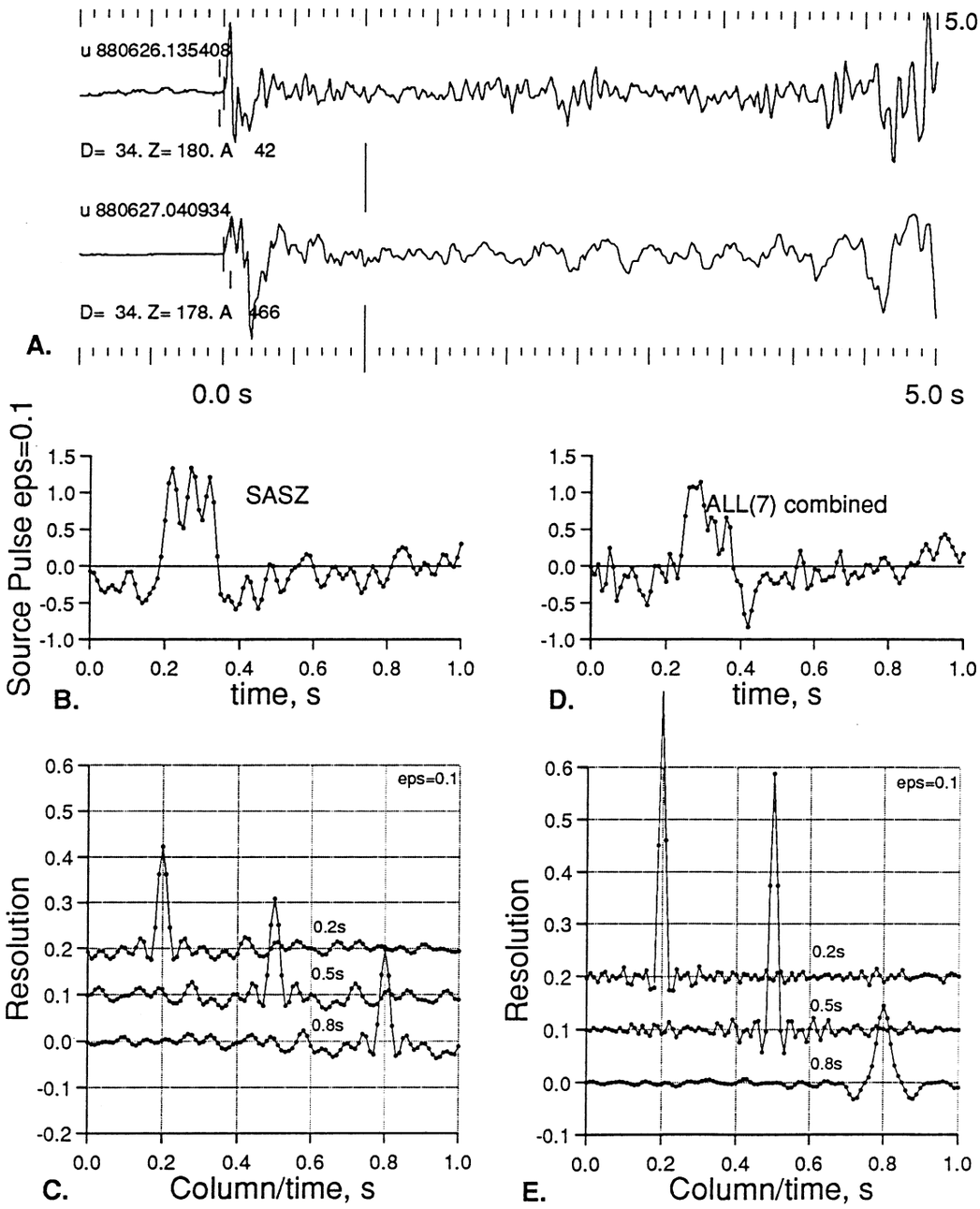

Figure 4. A. Example of a pair of seismograms from a colocated small (top) and large (bottom) event, recorded at station SAS (Sand Point) 34 km from the epicenter. Shumagin magnitudes are 1.9 and 2.7 for the top and bottom event. B. Resulting source pulse derived by time-domain deconvolution of the seismograms in A; only first second of P is used and signal-generated noise is assumed to be 10% of power in signal. C. Three selected rows in the resolution matrix for the inversion in B, corresponding to lags of 0.2, 0.5, and 0.8 s. A delta-function row with unit amplitude indicates that source pulse points are perfectly resolved; the width of the resolution rows indicate length of time over which true source pulse is being averaged to generate estimate in B. D. Same as B, except that 7 seismogram pairs are jointly inverted for a single source pulse (DLG, IVF, NGI, SASZ, and 3 components at SGB). The joint inversion averages over directivity effects; results of parameterized inversions show no systematic variation in rupture duration with azimuth or with distance. E. Same as C, for combined inversion.